Design of Ultra-Broadband Metamaterial Absorber with Ultra-Wide-Angle and Polarization Stability

Xianglin Kong, *Student Member, IEEE*, Lei Zhao, *Senior Member, IEEE*, Yun Zhou, and Zhongxiang Shen, *Fellow, IEEE*

***Abstract*—We investigate the underlying mechanisms of impedance mismatch under oblique incidence and propose a scan compensation method to design an ultra-broadband absorber with ultra-wide-angle and polarization stability. For realization, a dual-section dielectric layer is introduced to improve the input impedance, while magnetic material is primarily employed to mitigate frequency shift under oblique incidence, achieving much superior absorption performance of transverse electric and transverse magnetic waves at large incident angles. Integrating resistive surfaces, dielectric layers, and a grounded magnetic layer, an ultra-broadband and ultra-wide-angle microwave absorber is designed. Cube honeycomb structures are used to replace unavailable low-permittivity dielectrics to enable experimental validation. A prototype is fabricated, assembled and tested, and the measured results show that it achieves at least 90% absorption in 2.0-14.8 GHz under the normal incidence, with a fractional bandwidth of 152.38%. When the incident angle reaches 60°, the absorber maintains absorptivity at least 90% for both transverse electric and transverse magnetic waves. Measured results indicate that the designed absorber achieves ultra-broadband absorption performance with ultra-wide-angle and polarization stability.**

***Index Terms*—Absorber, effective medium theory, magnetic material, resistive surface.**

I. Introduction

An excellent absorber is characterized by ultra-broadband and good absorption with ultra-wide-angle and polarization stability. To achieve good absorption performance, its input impedance must match the free-space impedance at varying incident angles, so that the electromagnetic waves can enter the absorber and be dissipated. However, as the incident angle increases, the free-space impedance for transverse electric (TE) and transverse magnetic (TM) polarizations not only deviate from those at normal incidence, exhibiting distinctly divergent trends in opposite directions. This induces, compared to normal incidence, diminished absorptivity for TE polarization and shifted absorption bandwidth toward high frequencies for TM polarization. It is a great challenge to design an ultra-broadband absorber with ultra-wide-angle and polarization stability.

Traditional absorbing materials, such as Salisbury screen [1], Jaumann absorber [2] and Dallenbach structure [3] suffer from narrow bandwidth, fixed polarization and huge volume, which promote the study of novel absorbing structure with broadband absorption characteristic [4-6]. In general, ways to expand the bandwidth include loading lumped elements [7-11], resistive films [12-17] and stacking multi-layer structures [18-21]. For example, a low-profile wideband absorber based on metallic strips embedded with resistors was proposed to achieve at least 90% absorption from 2.77 GHz to 12.17 GHz [10]. An ultra-broadband multilayer absorber based on resistive film was designed to realize 90% absorption from 1.14 GHz to 14.2 GHz [12]. Unfortunately, the absorption of the aforementioned broadband absorbers does not surpass incident angle of 30°, which means that wide-angle characteristic needs further improvement.

Recently, efforts from matching dielectric layer [22-27], 3D structures [28-31], traditional multilayer structure (TMS) [32-35] and magnetic materials (MM) [36-38] were proposed to design ultra-broadband and ultra-wide-angle absorbers. For example, Munk et al. demonstrated that the input impedance can be compensated by placing a matching dielectric layer for oblique incidence [22]. Several absorbers based on single matching layer (SML) or dual-section matching layer (DML) were proposed to achieve -10 dB reflection coefficient under 45°TE-polarized wave incidence and 50° TM-polarized wave incidence [24,25,27]. To further improve the wide-angle performance, a near-omnidirectional metamaterial absorber was designed, which maintains 90% absorptivity under 82° TM-polarized wave oblique incidence [30]. However, it allows 90% absorptivity for TE-polarized wave within the incident angle less than 45°. It is worth noting that several studies have presented that magnetic material-based absorbers can achieve absorptivity above 90% at 60° under TM polarization, yet fail to exceed 45° under TE polarization [36,37]. The mentioned

This work was supported in part by the Fundamental Research Funds for the Central Universities under Grant 2023XSCX026, the Postgraduate Research & Practice Innovation Program of Jiangsu Province under Grant KYCX232707, the Graduate Innovation Program of China University of Mining and Technology under Grant 2023WLKXJ094, and the National Natural Science Foundation of China under Grant 61771226, *(Corresponding author: L. Zhao)*.

X. Kong, L. Zhao, and Y. Zhou are with the School of Information and Control Engineering, China University of Mining and Technology, Xuzhou, China (e-mail: xlkong@cumt.edu.cn, leizhao@cumt.edu.cn, yunzhou@cumt.edu.cn). Z. Shen is with Beijing Institute of Technology, Jiaxing, Zhejiang, China 314019 (e-mail: shenzx@bit.edu.cn).

approaches solely employing a single method are generally insufficient in improving the absorption performance for TE and TM polarizations at large incident angles. To further enhance wide-angle performance, a broadband absorber based on modified magnetic material was proposed to achieve at least -10 dB reflection coefficient under TE- and TM- polarized waves oblique incidence within 0-60° [38]. These studies have proposed absorbers exhibiting good absorption characteristics, but operating bandwidth and wide-angle characteristics need to be further improved, and the underlying mechanisms of impedance mismatch under oblique incidence need further exploration. So far, few absorbers have reported that can achieve ultra-broadband absorption performance with ultra-wide-angle and polarization stability.

In this paper, we investigate the underlying mechanisms of impedance mismatch under wide-angle oblique incidence and propose scan compensation method that employing magnetic material and a dual-section dielectric matching layer to jointly mitigate impedance mismatch for TE and TM polarizations at large incident angles. An ultra-broadband metamaterial absorber was designed by using the proposed method, and presents sufficient advantages compared with existing absorbers. The proposed design has the following features: (1) it provides a scan compensation method to mitigate polarization-sensitive limitations and unifies polarization stability for TE and TM waves at large incident angles; (2) the cube honeycomb is used to replace unavailable low-permittivity dielectrics in designing absorber to obtain a good performance; (3) it can achieve 90% absorptivity with the overlapping fractional bandwidth of 136.4% under incident angles from 0° at 60°.

II. Operating Principle

A. Free-Space Impedance Variation under Oblique Incidence

A single-layer lossy medium ($\varepsilon=\varepsilon'-j\varepsilon''$, $\mu=\mu'-j\mu''$) with the thickness of d is placed on a metallic plate to analyze the free-space impedance variation under oblique incidence. When an arbitrarily polarized plane wave is obliquely incident on the medium surface, the incident electric field can be resolved into two components [39]. One component is vertical to the incidence plane, referring to TE polarization. The other component is parallel to the plane of incidence, corresponding to TM polarization. Consequently, the analysis of the oblique incidence can be divided into TE and TM polarizations, as depicted in Fig. 1 (a). The free-space impedance of TE polarization and TM polarization can be expressed as

$$Z_0^{TE} = \frac{Z_0}{\cos\theta_0} \tag{1}$$

$$Z_0^{TM} = Z_0 \cos\theta_0 \tag{2}$$

where Z_0=377 Ω is the free-space impedance under the normal incidence, and θ_0 is the incident angle.

Fig. 1 (c) shows that the free-space impedances of TE and TM polarizations vary with the incident angle θ_0. As the incident angle θ_0 increases, $cos\theta_0$ decreases, leading to a significant increase of the free-space impedance for TE polarization and as well as a slow decrease for TM polarization.

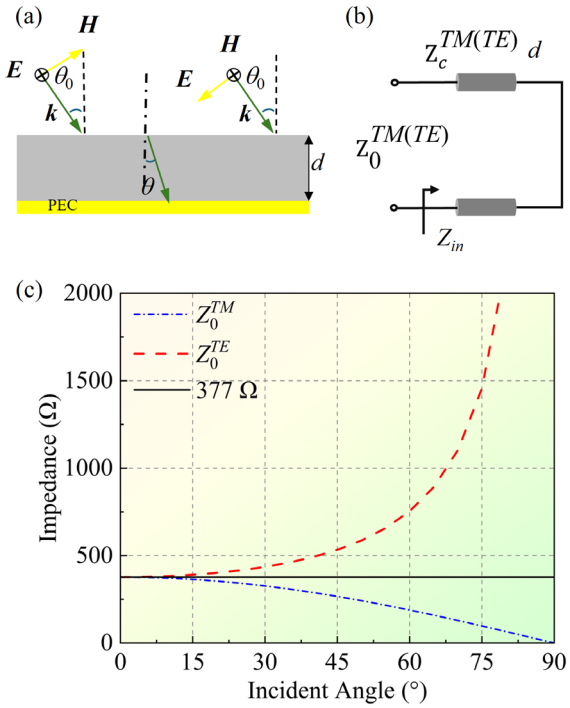

Fig. 1. (a) A grounded medium layer under TE and TM polarizations and its circuit model. (c) The free-space impedance at various incident angle.

This apparent opposite trend resulting in obtaining a good impedance matching for TE and TM polarizations at the same time seems to be impossible. Hence, it is a great challenge for an absorber to maintain good absorption performance under normal and oblique incidence simultaneously.

B. Input Impedance Variation under Oblique Incidence

When a plane wave is incident at an oblique angle upon an absorbing material, *i.e.*, $\theta_0>0$, the refraction angle θ is a complex quantity, which can be calculated by Snell's Law

$$\cos\theta = \sqrt{1-\frac{sin^2\theta_0}{\varepsilon\mu}} = |\cos\theta|e^{j\varphi} \tag{3}$$

where $|\cos\theta|$ and φ can be derived as [40]

$$|\cos\theta| = \sqrt{\frac{1}{\cos 2\varphi}\left(1-\frac{\cos\delta}{|\mu||\varepsilon|}sin^2\theta_0\right)} \tag{4a}$$

$$\varphi = \tan^{-1}\left(\frac{\sin\delta}{2\left(\cos\delta-\frac{|\mu||\varepsilon|}{sin^2\theta_0}\right)}\right) \tag{4b}$$

where δ is relative to the real and image part of μ and ε, which can be calculated by $\delta=\mu''/\mu'+\varepsilon''/\varepsilon'$.

The propagation constant γ of the medium can be written as

$$\gamma = \alpha + j\beta = j\frac{2\pi f}{c}\sqrt{\varepsilon\mu} \tag{5}$$

in which α and β are the attenuation and phase constants. The expression of α and β can be obtained by

$$\alpha = \frac{\sqrt{2}\pi f}{c}\sqrt{\sqrt{(\mu'\varepsilon'-\mu''\varepsilon'')^2+(\mu'\varepsilon''+\mu''\varepsilon')^2}-(\mu'\varepsilon'-\mu''\varepsilon'')} \tag{6a}$$

$$\beta = \frac{\sqrt{2}\pi f}{c}\sqrt{\sqrt{(\mu'\varepsilon'-\mu''\varepsilon'')^2+(\mu'\varepsilon''+\mu''\varepsilon')^2}+(\mu'\varepsilon'-\mu''\varepsilon'')} \tag{6b}$$

The electric field $\boldsymbol{E}_t$ in material can be expressed as

$$E_t = E_{t0}e^{-[\alpha_x x+j(\beta_x x+\beta_y y)]} \tag{7}$$

in which

$$\alpha_x = (\alpha\cos\varphi-\beta sin\varphi)|\cos\theta| \tag{8a}$$

$$\beta_x = (\alpha\sin\varphi+\beta cos\varphi)|\cos\theta| \tag{8b}$$

$$\beta_y = \beta_0\sin\theta_0 \tag{8c}$$

A succinct formula of the true refraction angle can be decomposed from the complex refraction angle θ as [40,41]

$$\psi = \tan^{-1}[\frac{\beta_y}{\beta_x}] = \tan^{-1}[\frac{1}{Re(cot\theta)}] \quad (9)$$

Note that the result ψ is a real number, its core contribution is used to analysis the trend in the electrical length under oblique incidence in this paper. If the product $|\mu||\varepsilon|$ is a sufficiently large value, $cos\theta$ becomes independent of the incident angle, implying that the refraction angle in medium is insensitive to the incident angle.

The characteristic impedance of TE and TM polarized waves under oblique incidence can be written as [39]

$$Z_c^{TE} = Z_0\sqrt{\frac{\mu}{\varepsilon}}\frac{1}{cos\theta} \quad (10)$$

$$Z_c^{TM} = Z_0\sqrt{\frac{\mu}{\varepsilon}}cos\theta \quad (11)$$

Moreover, the input impedance of the medium of TE and TM polarized waves under oblique incidence can be calculated by

$$Z_{in}^{TM(TE)} = Z_c^{TM(TE)}tanh(\gamma d cos\theta) \quad (12)$$

where in which c=3×10^8 m/s is the speed of wave propagating in free-space. Furthermore, the reflection coefficient of TE and TM polarized waves under oblique incidence can be described as

$$|\Gamma^{TM(TE)}| = |\frac{Z_{in}^{TM(TE)} - Z_0^{TM(TE)}}{Z_{in}^{TM(TE)} + Z_0^{TM(TE)}}| \quad (13)$$

In general, as incident angle increases, the absorption performance of a non-magnetic absorber exhibits a significant decline under TE-polarized waves, while demonstrating a gradual decline under TM-polarized waves. In both cases, the operating bandwidth shifts toward higher frequencies. The resonant frequency can be analyzed by the electric length of $\beta d cos\psi$~$\pi/2$ [22], to maintain the resonant condition, the frequency needs to be raised to compensate for the reducing $cos\psi$ as increasing incident angle. It leads to resonant frequency shifting to higher frequencies and the absorption bandwidth undergoes a corresponding offset. It is assumed that the input impedance of an absorber under the normal incidence is matched perfectly with the free-space impedance, *i.e.*, Z_0=Z_{in}. For TE polarization, the difference between the characteristic impedance Z_c^{TE} and free-space impedance Z_0^{TE} increase sharply as the incident angle increases. As a result, the input impedance is mismatched to the free-space impedance variation, thus the reflection coefficient increases significantly. For TM polarization, the difference between the characteristic impedance Z_c^{TM} and free-space impedance Z_0^{TM} increase flatly as the incident angle increases. Hence, the reflection coefficient shows a slow but tolerable deterioration. In summary, the root cause of this phenomenon lies in the fact that the characteristic impedance changes with a slower rate than the free-space impedance, which consequently exacerbates the impedance mismatch.

C. *Impedance Matching with Scan Compensation*

To achieve good wave absorption characteristics under wide-angle incidence, it is essential to overcome two main obstacles: the deterioration of reflection coefficient and frequency shift. Munk et al. proposed a method of scan compensation that

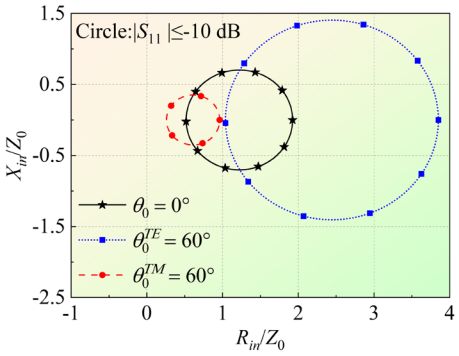

Fig. 2. Impedance matching circles for oblique incidence at θ_0=0°, θ_0=60° for TE and TM polarizations.

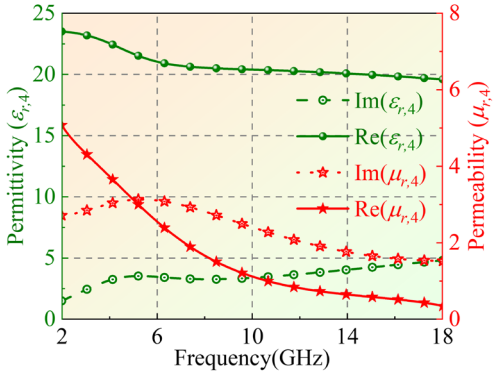

Fig. 3. Complex permittivity and permeability of commercial magnetic material.

places an impedance matching layer in front of an absorber to maintain absorption performance under wide oblique incident angle [22]. In addition, introducing the dual-section impedance-matching layers is a powerful method to improve large angle stability, because it can provide better impedance matching to compensate for impedance mismatch at large angle, thereby maintaining good absorption [23, 25]. The optimal permittivity of the top dielectric layer can be approximately given as [22]

$$\varepsilon_c \approx 1 + \cos\theta_0 \quad (14)$$

where θ_0 is the incident angle between the direction of propagation in air and the normal to absorber. A great deal of studies demonstrated that it is a feasible method to improve the oblique angle stability, especially for the absorption degradation problem at oblique incidence, but the problem of frequency shift needs to be further improved. When incident waves change from normal to oblique incidence, the value of $cos\psi$ will change from 1.0 to a value smaller than one. Consequently, f must increase to maintain $\beta d cos\psi \sim \pi/2$. Compared to non-magnetic absorbers (NMA), magnetic absorbers (MA) possess higher permeability and permittivity, demonstrating that the value of $cos\psi$ exhibits a smaller decrease as incident angle increases according Equation (3) and (4). Consequently, the frequency only needs to be shifted slightly towards high frequencies under large angle incidence, the resonance condition can be maintained. In conclusion, it is favorable to design an absorber with ultra-wide-angle characteristic by utilizing magnetic material and impedance matching layer.

D. Impedance Matching under Oblique Incidence

An absorber with good absorption under varying incident angles means that its input impedance needs to well match the free-space one. The impedance matching situation of absorbers is hard to obtain due to it is a transcendental equation with six parameters. To gain insight and comprehend the impedance matching condition more intuitively, we derive the impedance circles of various incident angles. An arbitrary absorber is equivalent to a single layer medium according to the effective medium theory. Its input impedance of TE and TM polarized waves under oblique incidence can be expressed as

$$Z_{in}^{TM(TE)} = R_{in}^{TM(TE)} + jX_{in}^{TM(TE)} \quad (15)$$

Substituting (15) into (13), the reflection coefficients of TE and TM polarized waves under oblique incidence can be further calculated by

$$\left|\Gamma^{TM(TE)}\right| = \left|\frac{R_{in}^{TM(TE)}+jX_{in}^{TM(TE)}-Z_0^{TM(TE)}}{R_{in}^{TM(TE)}+jX_{in}^{TM(TE)}+Z_0^{TM(TE)}}\right| \quad (16)$$

By simultaneously squaring and simplifying both sides of (16), a standard circle equation can be obtained by

$$\left(R_{in}^{TM(TE)}\right)^2 + \left(X_{in}^{TM(TE)}\right)^2 + \left(Z_0^{TM(TE)}\right)^2 + 2R_{in}^{TM(TE)}Z_0^{TM(TE)}\frac{\left|\Gamma^{TM(TE)}\right|^2+1}{\left|\Gamma^{TM(TE)}\right|^2-1} = 0 \quad (17)$$

Then the center and radii of the impedance circles are

$$O=\left(Z_0^{TM(TE)}\frac{\left|\Gamma^{TM(TE)}\right|^2+1}{\left|\Gamma^{TM(TE)}\right|^2-1},0\right),\ r^{TM(TE)}=Z_0^{TM(TE)}\sqrt{\left(\frac{\left|\Gamma^{TM(TE)}\right|^2+1}{\left|\Gamma^{TM(TE)}\right|^2-1}\right)^2-1},$$

respectively. That is, the impedance circles for TE and TM polarizations depend on the desired reflection coefficients $|\Gamma^{TM(TE)}|$ and incident angle θ_0. Fig. 2 presents impedance circles of normal incidence and oblique angle of 60° for TE and TM polarizations with $|S_{11}|$=-10 dB. As the incident angle increases, the range of impedance circle for TE polarization increases significantly, while for TM polarization shows reduction. The trends are consistent with the trends of the input impedance condition of TE and TM polarized waves under oblique incidence. If an absorber with desired reflection coefficient is to be obtain under oblique incidence, its input impedance must lie in the corresponding circle.

III. Results and Discussions

A. Physical Model and Equivalent Circuit Model

According to the scan compensation theory, an ultra-broadband absorber with ultra-wide-angle and polarization stability is designed by introducing dual-section matching layers and magnetic material. Wherein, the dual-section impedance matching layers is utilized to compensate the input impedance and magnetic material is employed to moderate the frequency shifts under oblique incidence for TE and TM polarization. To obtain 90% absorption under oblique incident angle of 60°, the permittivity of the top impedance matching layer can be calculated by equation (14) as $\varepsilon_{r,1}$=1.5. The other dielectric layers employed are polytetrafluoroethylene with relative permittivity of $\varepsilon_{r,2}$=$\varepsilon_{r,3}$=2.45, and the permittivity ($\varepsilon_{r,4}$) and permeability ($\mu_{r,4}$) of magnetic material are displayed in Fig. 3. Its imaginary parts of the permittivity and permeability are not zero, indicating that the magnetic material is lossy and can

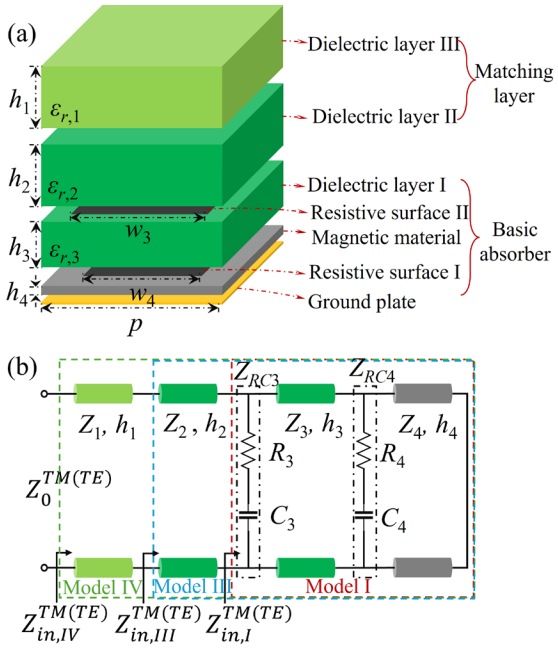

Fig. 4. An ultra-wide-angle absorber design. (a) The absorber structure and (b) its equivalent circuit model.

absorb electromagnetic waves. There is a large real part of the selected magnetic material and it should be insensitive to change in incident angle. As shown in Fig. 4, the physical model of the predicted absorber consists of a dual-section matching layer, magnetic material, resistive surface and conducting plate. Its equivalent circuit model can be established by using the transmission line theory. The magnetic material and dielectric layer can be represented as a transmission line of the same thickness, and the metallic plate can be considered as a short circuit. The array of square resistive surface can be considered as a series connection of a capacitance (C) and a resistance (R) [42,43]. The equivalent resistance is related to square resistance ($R_{s,i}$) and width (w_i) of resistive film and the period (p) of unit cell. The equivalent capacitances can be calculated by ε_{eff} times the corresponding C_0 values. Wherein, C_0 represents the equivalent capacitance of the resistive surface array in free space. The effective permittivity ε_{eff} depends on the dielectric environment surrounding the resistive surface. When a resistance is embedded in two substrates with different thickness (d_1, d_2) and different permittivity (ε_1, ε_2), ε_{eff} can be calculated by ε_{rd} = $(\varepsilon_1 d_1+\varepsilon_2 d_2)/(d_1+d_2)$ [44]. Fortunately, the values of R and C of TE and TM polarized waves under oblique incidence are equal to the ones under normal incidence, since the slight variations can be neglected [23]. This provides a possible way to understand absorption mechanism by establishing an equivalent circuit model under oblique incidence.

In the absorber design, impedance matching is complicated due to the fact that there exists a large number of structural parameters. In order to simplify the design difficulty, a method combining the equivalent circuit model and genetic algorithm is used to quickly obtain the desired reflection coefficient [16]. Because it constructs the closed-form relationships between lumped elements and absorber parameters. In this paper, the

optimization variables are h_1, h_2, h_3, h_4, w_3, w_4, $R_{s,3}$, and $R_{s,4}$. To quantify the deviation of the current iteration from the target, a fitness function is introduced as:

$$\text{F}itness = \sum_{i=1}^{m} \text{W}_i \times \sum_{j=1}^{\text{N}_i} \frac{|e_i(f_j)|^2}{\text{N}_i} \tag{18}$$

where i denotes the *i-th* optimization goal, W_i represents its associated weight. N_i and f_j correspond to the total number of frequency points and the specific frequency value for j-th point under the i-th goal, respectively. And $e_i(f_j)$ quantifies the discrepancy between the optimization response $R_i(f_j)$ and the desired threshold $G_i(f_j)$. The relationship is expressed as:

$$e_i(f_j)=\begin{cases} R_i(f_j)\text{-}G_i(f_j) & if\ R_i(f_j)>G_i(f_j) \\ 0 & if\ R_i(f_j)\le G_i(f_j) \end{cases} \tag{19}$$

where no contribution is made to the fitness function when $R_i(f_j)\le G_i(f_j)$, as the difference $e_i(f_j)$ is equal to zero. Finally, the target reflection coefficient is satisfied after 202iteration, taking 2min and15s, which run on a personal computer of a configuration with AMD Ryzen 7 7500G CPU @ 3.8 GHz and 16 GB RAM.

The transmission matrix of the basic absorber (model I) of TE and TM polarized waves under oblique incidence can be written as

$$\begin{bmatrix} A_I^{TM(TE)} & B_I^{TM(TE)} \\ C_I^{TM(TE)} & D_I^{TM(TE)} \end{bmatrix} = \begin{bmatrix} cos\,\delta_4 & jZ_4^{TM(TE)} sin\,\delta_4 \\ j\dfrac{sin\,\delta_4}{Z_4^{TM(TE)}} & cos\,\delta_4 \end{bmatrix} \begin{bmatrix} 1 & 0 \\ \dfrac{jwC_4}{1+jwC_4R_4} & 1 \end{bmatrix} \begin{bmatrix} cos\,\delta_3 & jZ_3^{TM(TE)} sin\,\delta_3 \\ j\dfrac{sin\,\delta_3}{Z_3^{TM(TE)}} & cos\,\delta_3 \end{bmatrix} \begin{bmatrix} 1 & 0 \\ \dfrac{jwC_3}{1+jwC_3R_3} & 1 \end{bmatrix} \tag{20}$$

To insight the contribution of the magnetic material, the transmission matrix of the basic absorber without magnetic material (model II) of TE and TM polarized waves under oblique incidence can be calculated by Equation (20).

Furthermore, the transmission matrix of the basic absorber with a single-section matching layer (model II) of TE and TM polarized waves under oblique incidence can be written as

$$\begin{bmatrix} A_{III}^{TM(TE)} & B_{III}^{TM(TE)} \\ C_{III}^{TM(TE)} & D_{III}^{TM(TE)} \end{bmatrix} = \begin{bmatrix} A_I^{TM(TE)} & B_I^{TM(TE)} \\ C_I^{TM(TE)} & D_I^{TM(TE)} \end{bmatrix} \begin{bmatrix} cos\,\delta_2 & jZ_2^{TM(TE)} sin\,\delta_2 \\ j\dfrac{sin\,\delta_2}{Z_2^{TM(TE)}} & cos\,\delta_2 \end{bmatrix} \tag{21}$$

Finally, the transmission matrix of the basic absorber with a dual-section matching layer (model IV) of TE and TM polarized waves under oblique incidence can be written as

$$\begin{bmatrix} A_{IV}^{TM(TE)} & B_{IV}^{TM(TE)} \\ C_{IV}^{TM(TE)} & D_{IV}^{TM(TE)} \end{bmatrix} = \begin{bmatrix} A_{III}^{TM(TE)} & B_{III}^{TM(TE)} \\ C_{III}^{TM(TE)} & D_{III}^{TM(TE)} \end{bmatrix} \begin{bmatrix} cos\,\delta_1 & jZ_1^{TM(TE)} sin\,\delta_1 \\ j\dfrac{sin\,\delta_1}{Z_1^{TM(TE)}} & cos\,\delta_1 \end{bmatrix} \tag{22}$$

where $Z_i^{TM(TE)}$ is the characteristic impedance of TE and TM polarized waves under oblique incidence, which can be calculated by

$$Z_i^{TE} = Z_0 \sqrt{\frac{\mu_{r,i}}{\varepsilon_{r,i}}} \frac{1}{cos\theta_i}, i = 1,2,3,4 \tag{23}$$

$$Z_i^{TM} = Z_0 \sqrt{\frac{\mu_{r,i}}{\varepsilon_{r,i}}} cos\theta_i, i = 1,2,3,4 \tag{24}$$

$$\delta_i = \frac{2\pi f}{c_0} \sqrt{\varepsilon_{r,i}\mu_{r,i}} h_i cos\,\theta_i, i = 1,2,3,4 \tag{25}$$

where $\mu_{r,i}$ and $\varepsilon_{r,i}$ are relative permeability and permittivity of the i-th layer medium of thickness h_i. The refraction angle θ_i in the i-th layer medium (i=1, 2, 3, 4,) can be derived by equation (3). R_i, C_i (i=3,4) are equivalent resistance and capacitance of the resistive films. Furthermore, the input impedance of model I, II, III and IV can be represented as

$$Z_{in,i}^{TM(TE)} = \frac{A_i^{TM(TE)} Z_L + B_i^{TM(TE)}}{C_i^{TM(TE)} Z_L + D_i^{TM(TE)}}, i = I, II\ III, IV \tag{26}$$

where Z_L =0 because of the short circuit.

After optimization, the structural parameters of the ideal absorber can be obtained as follows: h_4=1.09 mm, h_3=5 mm, h_2=h_1=6 mm, w_4=8.95 mm, w_3=9.04 mm, $R_{s,4}$=315.6 Ω/sq, $R_{s,3}$=201.6 Ω/sq. The absorber model is then constructed in full-wave simulator to calculate its reflection characteristics.

B. Simulation Results

In order to verify circuit calculation results, the proposed absorber model is built in the commercial electromagnetic simulation software and calculated using the frequency domain solver. For the oblique incidence case, the incidence angle of the electromagnetic wave is set in the Floquet port, and TE and TM modes are configured as the excitations. The boundary condition in the normal direction is set as "open (add space)", while the directions perpendicular to the normal are set as "unit cell" boundary conditions. To ensure simulation accuracy, the cells per wavelength is set to 15, and when incident angle is 0° (60°), the number of meshing cells are 92853 and 91666, the simulation time are 5 min 54 s and 5 min, and the iteration count to 17 and 14, respectively.

To illustrate the individual contribution of different layers, Fig.5 shows full-wave simulation and circuit calculation results of reflection coefficient and input impedance of model I, II, III and IV. By comparing the results of model I and II in Fig. 5(a) and (b), the reflection coefficient of model I at θ_0^{TM}=60°shows almost no shift for starting frequency compared to normal incidence and more wider operating bandwidth. Therefore, magnetic material contributes to expanding absorption performance and mitigating frequency shift. Besides, a grating lobe is observed on the full-wave simulation results of θ_0^{TM}=60° in Fig.(b), as marked in a red circle at 12.2 GHz. In Fig. (c), the bandwidth of model III is extended to 2.13-14.4 GHz at θ_0=0°. Its reflection coefficient at θ_0^{TM}=60° is less than -10 dB within 2.46-18 GHz, while fails to meet the condition of less than -10 dB at θ_0^{TE}=60°. As shown in Fig. 5(d), the reflection coefficient of model IV is less than -10 dB within 2.01-15.4 GHz at θ_0=0°. Its reflection coefficient can maintain below -10 dB from 2.68 to18 GHz at θ_0^{TE}=60°and from 2.54 to 17.5 GHz at θ_0^{TM}=60°. The overlapping bandwidth (OBW) for normal incidence, TE- and TM-polarized oblique incidence from 0° to 60° is 2.69-15.4 GHz. Fig. 5(e)-(h) illustrate the situation of input impedance of model I, II, III and IV at θ_0=0°, θ_0^{TE}=60° and θ_0^{TM}=60°, respectively. The input impedance of the designed absorber with dual-section matching layer and magnetic material lies in the impedance circle with $|S_{11}|\le$-10 dB of θ_0=0°, θ_0^{TE}=60° and θ_0^{TM}=60°, indicating that its input impedances match with the free-space ones. In conclusion, the proposed scan compensation method is feasible to design ultra-broadband absorbers with ultra-wide-angle and polarization-stability.

Moreover, the grating lobes of periodic structure can be calculated by $f_{GL}=nc_0/(p(\sin\theta_0+1))$ [30], where p=12 mm is the period of unit cell, c_0 is the speed of electromagnetic wave in

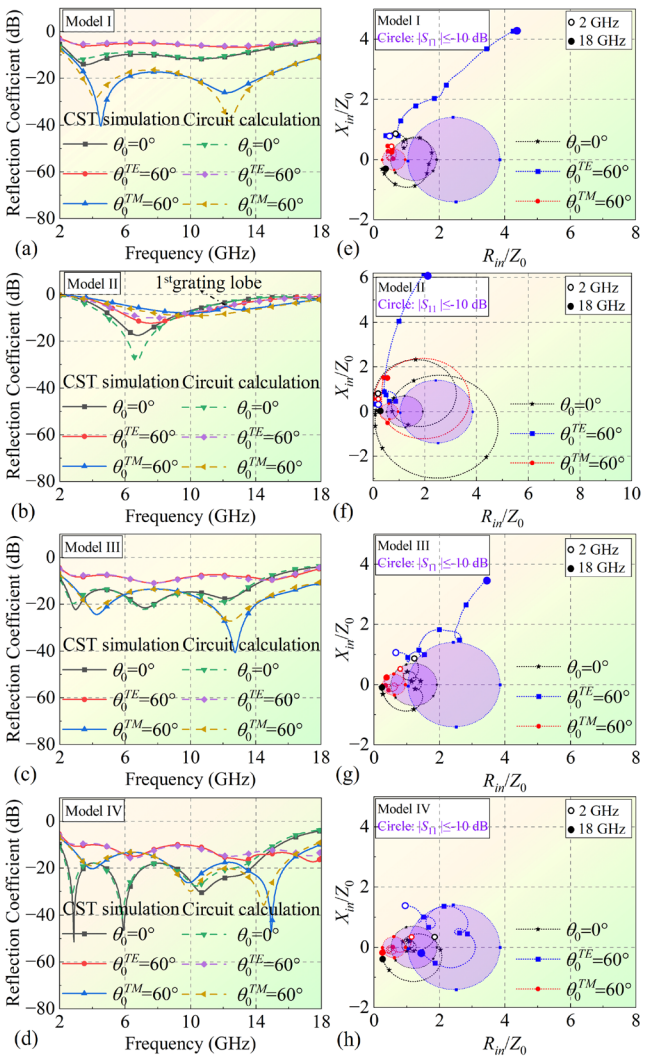

Fig. 5. Simulation results of reflection coefficient and input impedance under TE- and TM-polarized waves incidence. (a)-(d) Comparison for reflection coefficient CST simulation and circuit calculation of Model I, II, III and IV at incident angle of θ_0=0°, θ_0^{TE}=60° and θ_0^{TM}=60°. (e)-(h) Input impedance of model I, II, III and IV at incident angle of θ_0=0°, θ_0^{TE}=60° and θ_0^{TM}=60°.

vacuum, n=1 or 2 is the order of grating lobe, and f_{GL} is the frequency of grating lobe. According to the mentioned equation, the first-order grating lobe under normal incidence should occur at about 25 GHz. When incident angle is 60°, the first-order grating lobe should occur at about 13.4 GHz, and the second-order grating lobe should occur at about 26.8 GHz. The full-wave simulation results of reflection coefficient at θ_0=0°, θ_0^{TE}=60° and θ_0^{TM}=60° show no grating lobe in operating band and are consistent with circuit calculation results, indicating that the proposed absorber can avoid the generation of grating lobe.

To insight physical mechanism of improving performance at large incident angle of 60°. As shown in Fig. 6, the distribution of magnitude of E-field(|$\boldsymbol{E}$|) and H-field(|$\boldsymbol{H}$|) in xoz plane at 10 GHz, under condition of normal incidence and oblique incidence of 60° TE- and TM- polarized waves. In Fig. 6(a) and (b), the distribution of |$\boldsymbol{E}$| and |$\boldsymbol{H}$| shows that there is no standing wave generated under normal incidence. As shown in Fig. 6(c)-(f), the distribution of |$\boldsymbol{E}$| and |$\boldsymbol{H}$| transition

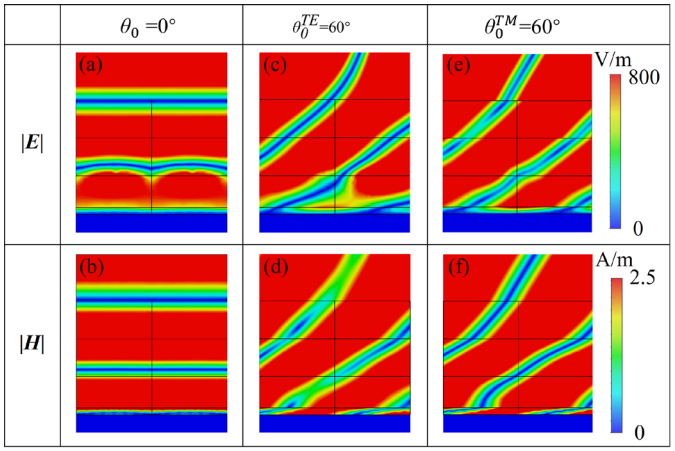

Fig. 6. The distribution of |$\boldsymbol{E}$| and |$\boldsymbol{H}$| under normal incidence and oblique incidence of 60° TE- and TM- polarized waves. (a), (b) Distribution of |$\boldsymbol{E}$| and |$\boldsymbol{H}$| at θ_0=0°. (c), (d) Distribution of |$\boldsymbol{E}$| and |$\boldsymbol{H}$| at θ_0^{TE}=60°. (e), (f) Distribution of |$\boldsymbol{E}$| and |$\boldsymbol{H}$| at θ_0^{TE}=60°.

smoothly in absorber, particularly through the dual-section matching layer, providing that it has good impedance matching characteristics and that the matching layer can improve impedance matching at θ_0^{TE}= θ_0^{TM}=60°. In Fig. 6(e) and (f) the distribution of |$\boldsymbol{H}$| in magnetic material occurs deflection phenomenon at θ_0^{TE}= θ_0^{TM}=60°, meaning that the incident angle decreases. It contributes to maintaining absorbing resonant condition and minimizing frequency shift, thereby mitigating the mismatch under large-angle incidence. Therefore, the dual-section layer and magnetic substrate jointly mitigate TE and TM mismatch.

Introducing a matching layer on the basic absorber can effectively improve the absorption characteristics under oblique incidence. However, it is hard to obtain the desired dielectric slab with low permittivity of $\varepsilon_{r,1}$=1.5 in practice. Fortunately, it can be obtained by the homogenization method based on the effective medium theory. In theory, it can obtain accurate equivalent permittivity only when the periodic cell size is sufficiently small compared to the operating frequency wavelength, i.e., D<1/2λ [45]. The cube honeycomb structures are used to replace the uniform dielectric slab in experimental stage, as shown in Fig. 7(a). Fig. 7(b) and Fig. 7 (c) show a top and side views of the unit cell of cube honeycomb structure. Its effective permittivity can be represented by a tensor form, the effective radial permittivity ε_t and axial permittivity ε_z can be calculated by [46,47]

$$\varepsilon_t = \varepsilon_a \frac{(2-g)\varepsilon_0 + g\varepsilon_a}{g\varepsilon_0 + (2-g)\varepsilon_a} \quad (27)$$

$$\varepsilon_z = \varepsilon_0 + (1-g)\varepsilon_a \quad (28)$$

where ε_a is the relative permittivity of the dielectric material for constructing the cube honeycomb, ε_0 is the relative permittivity of the fill materials and its fill factor g is given by g=1-((D-2r)/D)^2.

Therefore, the effective permittivity can be controlled by changing the constructing dielectric material. The permittivity of dielectric layer is ε_a=2.65, then D=6 mm, r=0.65 mm, ε_t≈1.5 and ε_z≈1.63. This means that the effective permittivity increases from 1.5 to 1.63 with incident angle ranging from 0° to 90°.

Figs. 7(e) and (f) show the absorptivity at various incidence

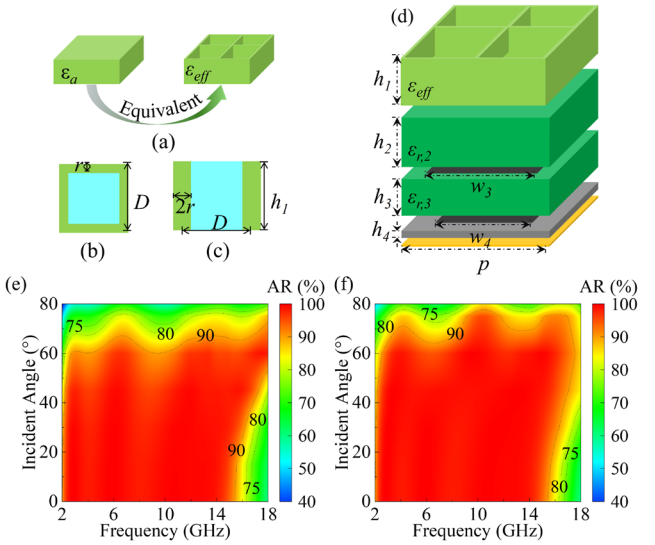

Fig. 7. The equivalent absorber and its absorption. (a) The diagram of cube honeycomb structures, (b) The top and (c) side view of unit cell of cube honeycomb structure, (d) The simulation absorptivity under oblique incidence for (e) TE polarization and (f) TM polarization.

angles for TE and TM polarizations. For TE polarization, the proposed absorber can achieve more than 90% absorptivity within 2.01-15.4 GHz under the normal incidence. As the incidence angle increases for TE polarization, the absorptivity decreases and a slight shift toward high frequencies is noted, but still maintains about 90% absorption in 2.69-15.4 GHz at θ_0= 60°. In the operating bandwidth, its absorption is more than 90%. For TM polarization, the starting frequency at oblique incidence is slightly shifted towards high frequencies compared to the normal incidence, and still maintains more than 90% absorption within 2.54-15.4 GHz at θ_0= 60°. However, when the incidence angle increases to 75°, the absorptivity for TM polarization remains at approximately 80%, while that for TE polarization drops to 70%. The overlapping fraction bandwidth of the normal incidence and oblique incidence at θ_0= 60° for TE and TM polarizations is 140.52%. In summary, the designed absorber possesses good impedance characteristics and ultra-broadband absorption performance with ultra-wide-angle and polarization stability.

C. Experimental Validation

In order to validate the proposed method, a sample with dimension of 300 mm×300 mm and 18.14 mm thickness is fabricated and measured. It consists of resistive surfaces, dielectric slab, magnetic material and cube honeycomb Resistive surfaces fabricated using screen-printing techniques are adhered to polyimide films with a thickness of 0.025 mm (dielectric constant of 3.0-j0.003). The cube honeycomb structures consist of several small dielectric slabs with relative permittivity of 2.6 manufacturing high-precision laser cutting technology. Magnetic material is a commercial product, which offers stable performance. Compared to non-magnetic absorber, magnetic materials are more expensive and heavier, but can mitigate impedance mismatch and achieve large-angle stability. These mature processes and materials to enable absorption performance testing.

The arch method is performed in a microwave anechoic chamber to measure the reflection coefficients of the sample, as shown in Figs. 8(a) and (b). Two pairs of broadband horn antennas are adopted to connect to the vector network analyzer (Keysight E5063A) as the transmitter and receiver. The two antennas operate in the frequency range of 2-18 GHz (LB-20180-SF). In measurements, the distance (L_{as}) between the antennas and the sample needs to satisfy the far-field condition, i.e., $L_{as} > 2D_a^2/\lambda$, where D_a is the diameter of the proposed sample. A metallic plate of the same dimension as the fabricated sample is used as a reference to perform the calibration of the reflection parameters of the absorber sample. Fig. 8(c) and (d) show the measured absorptivity of the absorber under oblique incidence of TE and TM polarizations within 2-18 GHz. It can achieve more than 90% absorption from 2 GHz to 14.8 GHz under the normal incidence. At incidence angle of 60°, it can maintain more than 90% absorption within 2.94-18 GHz for TE polarization and within 2.45-17.66 GHz for TM polarization. The OFWB shifts only 18.7% compared with the largest bandwidth of normal incidence, TE- and TM-polarized oblique incidence from 0° to 60°. There is a discrepancy in operating bandwidth between the measured results and simulation results under normal and oblique incidence. It may be caused by the machining tolerance coming from the effective cube honeycomb and magnetic material in the prototype. Overall, the proposed absorber can realize good absorption with ultra-wide-angle and polarization stability within ultra-broadband frequencies.

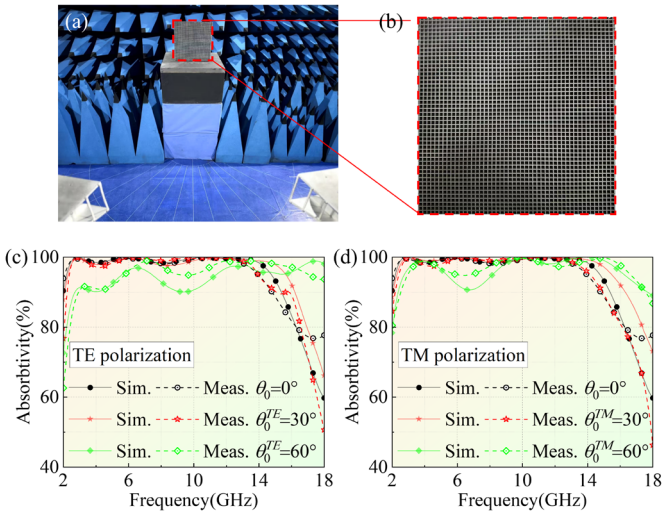

Fig. 8. Test configuration and measured results. (a) Test configuration in a microwave anechoic chamber, (b)Front view of the proposed absorber, Measured absorptivity under oblique incidence for (c) TE polarization and (d) TM polarization.

D. Comparison and Discussion

In order to illustrate the relation between absorption performance and thickness, an indicator of the causality ratio is defined by $R_c=h_t/h_{min}$ to evaluate the proposed absorber. In magnetic absorber, h_t is effective thickness calculated by $h_t=\Sigma_i\mu_i h_i$, where μ_i, h_i are the maximum value of the real part of permeability and thickness of the i-th layer material [49]. According to the Rozanov limit [48], the relationship between minimum thickness and bandwidth for absorber under can be expressed as

TABLE I
COMPARISON OF THE PROPOSED ABSORBER AND OTHER REPORTED ABSORBERS

Ref.	BW(GHz) (≥90% absorptivity) /FBW(%)				OBW(GHz) /OFBW(%)	Δ_{FBW}	Overall thickness	t/λ_L	R_c	Realization
	θ_0=0°	θ_0^{TE}&θ_0^{TM}	TE	TM						
[24]	2.79-20.62/152.3	50°	3.47-22/ 145.5	3.64-21.72/142.6	3.64-20.62/140	12.3%	12.53 mm	0.116	1.42	SML
[25]	2.7-14/135.3	45°	2.35-14/142.5	3.25-14/124.6	3.25-14/124.6	10.7%	18 mm	0.162	2.80	DML
[26]	2.5-18/157.9	30°	2-18/160	2-18/160	2.5-18/157.9	2.1%	12.7 mm	0.32	1.42	SML
[27]	2.98-18/143.2	50°	3.39-18/136.6	4.99-18/113.2	4.99-18/113.2	30%	8 mm	0.08	1.28	SML
[28]	0.63-6.55/164.9	45°	0.69-6.75/162.9	0.75-6.22/156.9	0.75-6.22/156.9	8%	60.2 mm	0.15	1.65	3D
[30]	1.5-4.5/103.3	45°	2.13-5/80.5	1.55-5/105.3	2.13-4.5/71.5	33.8%	22 mm	0.11	1.56	3D
[31]	2.11-3.89/59.3	50°	2.29-4.17/58.2	2.2-3.78/52.8	2.29-3.78/49.1	10.2%	13 mm	0.091	1.58	3D
[32]	2 -23/168	45°	2.39-18/153.1	3.3-18/138	3.3-18/138	30%	15.4 mm	0.102	1.47	Multilayer
[33]	1.08-5.9/137.1	45°	1.34-6.45/131.2	1.7-6.59/118	1.7-5.9/110.5	26.6%	29.4 mm	0.106	1.21	Multilayer
[38]	2.4-7.3/101	60°	3.43-8.38/83.8	2-10/133.3	3.43-7.3/72.1	61.2%	12.4 mm	0.10	2.04	Modified MM
This work	2-14.8/152.4	60°	2.94-18/143.8	2.45-17.6/151.1	2.94-14.8/133.7	18.7%	18.14 mm	0.121	1.48	DML & MM

$$h_{min} = \frac{\left|\int_{min}^{max} ln|\rho(\lambda)|d\lambda\right|}{2\pi^2} \approx \frac{\left|\int_{min}^{max}|\Gamma(\lambda)|d\lambda\right|}{172} \quad (29)$$

where $\rho(\lambda)$ and $\Gamma(\lambda)$ are a function of wavelength of reflection coefficient in linear and dB version. But the starting frequency and stopping frequency of the operating bandwidth with 90% absorptivity are used as upper and lower integration limits to better visualize the thickness performance. The causality ratio of the proposed absorber is 1.48, which is

Table I performs a comparison between our proposed design and other reported absorbers for incident angle, bandwidth (BW), fractional bandwidth (FBW), overlapping bandwidth OBW, OFBW, NP_A, overall thickness, causality ratio, and realization. The FBW can be calculated by $2\times(f_{max}-f_{min})/(f_{max}+f_{min})$, where f_{max}, f_{min} are the highest and lowest frequencies, respectively. The OFBW can be derived from the intersection of operating bandwidth of normal incidence and oblique incidence of TE and TM polarizations. Each of the aforementioned absorbers has its own unique advantages and disadvantages, making them suitable for various application scenarios. Comparison results indicate that it is difficult to achieve 90% absorptivity using a single method under wide-angle oblique incidence of TE- and TM-polarized waves. The proposed absorber combining DML and MM exhibits superior performance compared to other reported absorbers in term of BW, OFBW, Δ_{FBW}, causality ratio, and angle stability. Compared to non-magnetic absorber, magnetic materials are more expensive and heavier, but can mitigate impedance mismatch and achieve large-angle stability. According to the Rozanov limit, its overall thickness is close to the theoretical minimum thickness, and its relative thickness is comparable to that of existing absorbers. The proposed absorber offers significant advantages such as broadband bandwidth, large-angle stability, good absorptivity. It provides a potential solution for an absorber with broadband, large-angle stability and polarization stability in real-word application.

IV. CONCLUSION

In this paper, we have proposed a novel scan angle compensation method by introducing dual-section matching dielectric layers and magnetic materials. The dual-layer matching dielectric layers are primarily employed to improve the input impedance for TE-polarized and TM-polarized oblique incidence, thereby enhancing the absorption performance. Meanwhile, magnetic materials are utilized to mitigate oblique incidence-induced electrical length variations, thereby effectively suppressing the resultant frequency shift phenomenon. An absorber has been designed and measured to validate the effectiveness of the proposed method. The simulated and measured results demonstrate that our presented absorber can realize 90% absorption for both TE and TM polarizations within the incidence range of 0°-60°. The input impedance of the absorber is well matched to the free-space impedance across the incidence angles ranging from 0° to 60°. It indicates that the proposed scan angle compensation method is feasible for designing absorbers providing good absorption with excellent angle and polarization stability in ultra-broadband frequencies.

REFERENCES

[1] R. L. Fante and M. T. Mccormack, "Reflection properties of the Salisbury screen," *IEEE Trans. Antennas Propag.*, vol. 36, no. 10, pp. 1443-1454, Oct. 1988.

[2] L. J. Du Toit, "The design of Jauman absorbers," *IEEE Antennas and Propag. Mag.*, vol. 36, no. 6, pp. 17-25, Dec. 1994.

[3] D. L. Jaggard, N. Engheta, and J. Liu, "Chiroshield: a Salisbury/Dallenbach shield alternative," *Electron. Lett.*, vol. 26, no. 17, pp. 1332-1334, Aug. 1990.

[4] X. Zeng, X. Cheng, R. Yu, and G. D. Stucky, "Electromagnetic microwave absorption theory and recent achievements in microwave absorbers," *Carbon*, vol. 168, pp. 606-623, Oct. 2020.

[5] L. Wu, S. Shi, G. Wang, P. Mou, X. Liu, J. Liu, L. Liang, and C. Du, "Carbon nanocoils/carbon foam as the dynamically frequency-tunable microwave absorbers with an ultrawide tuning range and absorption bandwidth," *Adv. Funct. Mater.*, vol. 32, no. 52, p. 2209898, Dec. 2022.

[6] S. Ghosh, S. Sharma, W. Li, A. Nozariasbmarz, L. Raman, N. Liu, G. K. Goyal, Y. Zhang, S. E. Perini, M. Lanagan, S. Priya and B. Poudel,

"Broadband and tunable microwave absorption properties from large magnetic loss in Ni–Zn ferrite," *Adv. Mater. Technol.*, vol. 9, no. 6, p. 2301857, Mar. 2024.

[7] J. Qin, M. Sun, M. Wang, M. Guan, and A. Chen, "A hierarchical impedance matching approach for ultrawideband absorbers with wide angular stability," *IEEE Trans. Antennas Propag.*, vol. 72, no. 5, pp. 4116-4128, May. 2024.

[8] Z. Cao, H. Li, Y. Wu, G. Yao, Y. Zhao, Z. Huang, S. Guo, L, Miao and J. Jiang, "Backend-balanced-impedance concept for reverse design of ultra-wideband absorber," *IEEE Trans. Antennas Propag.*, vol. 70, no. 11, pp. 11217-11222, Nov. 2022.

[9] M. Lee, J. Park, K. Kim, J. Kim, E. Park and S. Lim, "Broadband and wide-incidence-angle transparent metamaterial absorber using eight-resistive-arm cell," *IEEE Antennas Wirel. Propag. Lett.*, vol. 23, no. 6, pp. 1754-1758, Jun. 2024.

[10] B. Zhang, C. Jin, and Z. Shen, "Low-profile broadband absorber based on multimode resistor-embedded metallic strips," *IEEE Trans. Microw. Theory Tech.*, vol. 68, no. 3, pp. 835-843, Mar. 2020.

[11] Z. Yao, S. Xiao, Z. Jiang, L. Yan, and B. Wang, "On the design of ultrawideband circuit analog absorber based on quasi-single-layer FSS," *IEEE Antennas Wirel. Propag. Lett.*, vol. 19, no. 4, pp. 591-595, Apr. 2020.

[12] T. Shi, M. Tang, J. Yang, and X. Yuan, "A low-profile and ultrawideband capacitive circuit absorber empowered by enlarged unit periodicity," *IEEE Antennas Wirel. Propag. Lett.*, vol. 21, no. 3, pp. 551-555, Mar. 2022.

[13] F. Y. Dong, C. Niu, M. Zhang, A. Wang, K. Duan, J. Zhao, W. Zhu and Z. Hou, "A lightweight ultra-wideband metasurface microwave absorber," *Adv. Mater. Technol.*, vol. 10, no. 7, p. 2401493, Apr. 2025.

[14] Y. Li, P. F. Gu, Z. He, Z. Cao, J. Cao, K. W. Leung and D. Ding, "An ultra-wideband multilayer absorber using an equivalent circuit-based approach," *IEEE Trans. Antennas Propag.*, vol. 70, no. 12, pp. 11911-11921, Dec. 2022.

[15] P. Chen, X. Kong, J. Han, W. Wang, K. Han, H. Ma, L. Zhao and X. Shen, "Wide-angle ultra-broadband metamaterial absorber with polarization-insensitive characteristics," *Chin. Phys. Lett.*, vol. 38, no. 2, pp. 27105-27801, Jan. 2021.

[16] X. Kong, S. Zhang, X. Pang, Y. Fu, L. Zhao and Z. Shen, "Fast design of ultrawideband absorbers based on equivalent circuit model," *IEEE Antennas Wirel. Propag. Lett.*, vol. 23, no. 6, pp. 1869-1873, Jun. 2024.

[17] X. Kong, H. Ma, P. Chen, C. Liang, W. Wang, K. Han, S. Zhang, X. Liu, L. Zhao and X. Shen, "Design of ultra-wideband metamaterial absorber based on resistance films," *Chinese Journal of Radio Science*, vol. 36, no. 6, pp. 947-952, Dec. 2021.

[18] Q. An, D. Li, W. Liao, T. Liu, D. Joralmon, X. Li and J. Zhao, "A novel ultra-wideband electromagnetic-wave-absorbing metastructure inspired by bionic gyroid structures," *Adv. Mater.*, vol. 35, no. 26, p. 2300659, Jun. 2023.

[19] J. Qin, Y. Gao, W. Zhang, S. Xiong, and W. Zhu, "Microfluidic metasurface with constant absorption efficiency throughout the Ku band," *Adv. Mater. Technol.*, vol. 9, no. 9, p. 2302145, May 2024.

[20] W. Wang, A. Wang, J. Liang, Z. Wang, J. Jiang, C. Xu, Y. Li, J. Wang and S. Qu, "Design and analysis of a wideband and wide angle 3D metamaterial absorber," *J. Phys. D-Appl. Phys.*, vol. 55, no. 32, p. 325302, Aug. 2022.

[21] N. Qu, G. Xu, Y. Liu, M. He, R. Xing, J. Gu and J. Kong, "Multi-scale design of metal–organic framework metamaterials for broad-band microwave absorption," *Adv. Funct. Mater.*, vol. 35, no. 18, p. 2402923, May 2025.

[22] B. A. Munk, P. Munk, and J. Pryor, "On designing Jaumann and circuit analog absorbers (CA absorbers) for oblique angle of incidence," *IEEE Trans. Antennas Propag.*, vol. 55, no. 1, pp. 186-193, Jan. 2007.

[23] A. Kazemzadeh and A. Karlsson, "Multilayered wideband absorbers for oblique angle of incidence," *IEEE Trans. Antennas Propag.*, vol. 58, no. 11, pp. 3637-3646, Nov. 2010.

[24] Z. Sun, L. Yan, X. Zhao, and R. X. Gao, "An ultrawideband frequency selective surface absorber with high polarization-independent angular stability," *IEEE Antennas Wirel. Propag. Lett.*, vol. 22, no. 4, pp. 789-793, Apr. 2023.

[25] F. He, K. Si, R. Li, D. Zha, J. Dong, L. Miao, S. Bie and J. Jiang, "Broadband frequency selective surface absorber with dual-section step-impedance matching for oblique incidence applications," *IEEE Trans. Antennas Propag.*, vol. 69, no. 11, pp. 7647-7657, Nov. 2021.

[26] X. Bai, Z. Mei, J. Zhang, W. Xu, W. Lin and T. Niu, "An ultrawideband, wide-angle, and transparent microwave absorber using indium tin oxide conductive films," *IEEE Antennas Wirel. Propag. Lett.*, vol. 23, no. 5, pp. 1543-1547, May 2024.

[27] Z. Ma, C. Jiang, W. Cao, J. Li, and X. Huang, "An ultrawideband and high-absorption circuit-analog absorber with incident angle-insensitive performance," *IEEE Trans. Antennas Propag.*, vol. 70, no. 10, pp. 9376-9384, Oct. 2022.

[28] S. Kim and S. Nam, "Ultra-wideband and wide-angle insensitive absorber based on TCDA-under-tightly coupled dipole array," *IEEE Trans. Antennas Propag.*, vol. 69, no. 9, pp. 5682-5690, Sep. 2021.

[29] J. Yadav, M. Saikia, K. V. Srivastava, and J. Ramkumar, "Three-dimensional rotation of FSS unit cell in broadband microwave absorber for large oblique incidence response," *IEEE Trans. Electromagn. Compat.*, vol. 65, no. 5, pp. 1320-1328, Oct. 2023.

[30] T. Shi, M. C. Tang, D. Yi, L. Jin, M. Li, J. Wang and C. W. Qiu, "Near-omnidirectional broadband metamaterial absorber for TM-polarized wave based on radiation pattern synthesis," *IEEE Trans. Antennas Propag.*, vol. 70, no. 1, pp. 420-429, Jan. 2022.

[31] T. Shi, L. Han, M. C. Tang, H. X. Xu and C. W. Qiu, "Dispersion-engineered, broadband, wide-angle, polarization-independent microwave metamaterial absorber," *IEEE Trans. Antennas Propag.*, vol. 69, no. 1, pp. 229-238, Jan. 2021.

[32] M. Gao, Q. Chen, Y. Zheng, L. Ding, D. Liao and Y. Fu, "Ultrabroadband absorber based on layered inkjet-printing resistive film," *IEEE Antennas Wirel. Propag. Lett.*, vol. 22, no. 2, pp. 228-232, Feb. 2023.

[33] Z. Yao, S. Xiao, Y. Li, and B. Wang, "Wide-angle, ultra-wideband, polarization-independent circuit analog absorbers," *IEEE Trans. Antennas Propag.*, vol. 70, no. 8, pp. 7276-7281, Aug. 2022.

[34] I. V P, S. V P, V. C, and S. Kumar T R, "Design of broadband circuit analog absorber with optimal thickness for stable angular response in c, x, ku, and k bands," *IEEE Trans. Electromagn. Compat.*, vol. 65, no. 6, pp. 2065-2069, Dec. 2023.

[35] Z. Wang, J. Huang, D. Sun, Q. Zeng, M. Song and T. A. Denidni, "UWB frequency-selective surface absorber based on graphene featuring wide-angle stability," *Sensors*, vol. 23, no. 5, p. 2677, Mar. 2023.

[36] M. I. Hossain, N. Nguyen-Trong, and A. M. Abbosh, "Broadband magnetic absorber based on double-layer frequency-selective surface," *IEEE Trans. Antennas Propag.*, vol. 70, no. 1, pp. 410-419, Jan. 2022.

[37] X. Kong, J. Liu, L. Zhao, H. Song, and S. Zhang, "A low-frequency ultra-wideband absorber based on multi-mechanism collaborative design (in Chinese)," *Sci. Sin Inform.*, vol. 54, no. 12, pp. 2868-2880, 2024.

[38] W. Yu, Y. Du, W. Wang, Q. Tan, L. Liu and G. Luo, "Broadband absorber with high angular stability based on magnetic material," *IEEE Trans. Antennas Propag.*, vol. 72, no. 7, pp. 6123-6128, Jul. 2024.

[39] D. K. Cheng, *Field and Wave Electromagnetics*, Addison-Wesley, Reading, MA, USA 1989.

[40] A. G. D'Aloia, M. D'Amore and M. S. Sarto, "Oblique Incidence Optimal Design of Microwave Dielectric-Magnetic Absorbing Composites," *IEEE Trans. Magn.*, vol. 58, no. 5, pp. 1-7, May 2022.

[41] Y. Liu, J. Qian, and Y. Tian, "Succinct formulas for decomposition of complex refraction angle," *in IEEE Antennas Propag. Soc. Int. Symp. Dig. Held Conjunct: USNC/CNC/URSI North Amer. Radio Sci. Meeting,* Columbus, OH, USA, Jun. 2003, pp. 487–490.

[42] F. Costa and A. Monorchio, "Closed-form analysis of reflection losses in microstrip reflectarray antennas," *IEEE Trans. Antennas Propag.*, vol. 60, no. 10, pp. 4650-4660, Oct. 2012.

[43] F. Costa, A. Monorchio, and G. Manara, "Analysis and design of ultrathin electromagnetic absorbers comprising resistively loaded high impedance surfaces," *IEEE Trans. Antennas Propag.*, vol. 58, no. 5, pp. 1551-1558, May 2010.

[44] F. Costa, A. Monorchio, and G. Manara, "Efficient analysis of frequency-selective surfaces by a simple equivalent-circuit model," *IEEE Antennas Propag. Mag.*, vol. 54, no. 4, pp. 35-48, Aug. 2012.

[45] M. Johansson, C. L. Holloway, and E. F. Kuester, "Effective electromagnetic properties of honeycomb composites, and hollow-pyramidal and alternating-wedge absorbers," *IEEE Trans. Antennas Propag.*, vol. 53, no. 2, pp. 728-736, Feb. 2005.

[46] E. F. Kuester and C. L. Holloway, "A low-frequency model for wedge or pyramid absorber arrays-i: theory," *IEEE Trans. Electromagn. Compat.*, vol. 36, no. 4, pp. 300-306, Nov. 1994.

[47] E. F. Kuester and C. L. Holloway, "Comparison of approximations for effective parameters of artificial dielectrics," *IEEE Trans. Microw. Theory Tech.*, vol. 38, no. 11, pp. 1752-1755, Nov. 1990.

[48] K. N. Rozanov, "Ultimate thickness to bandwidth ratio of radar absorbers," *IEEE Trans. Antennas Propag.*, vol. 48, no. 8, pp. 1230-1234, Aug. 2000.

Xianglin Kong received the M.S. and Ph. D. degree in information and communication engineering from China University of Mining and Technology, Xuzhou, China, in 2021 and 2025, respectively. He joined the Suqian University, Suqian, China, in 2026.
His research interests include microwave absorber, frequency selective surfaces.

Lei Zhao (Senior Member, IEEE) received the B.S. degree in mathematics from Jiangsu Normal University, Xuzhou, China, in 1997, and the M.S. degree in computational mathematics and the Ph.D. degree in electromagnetic fields and microwave technology from Southeast University, Nanjing, China, in 2004 and 2007, respectively. From 2007 to 2009, he worked with the Department of Electronic Engineering, The Chinese University of Hong Kong, Hong Kong, as a Research Associate. From 2009 to 2018, he worked with Jiangsu Normal University. During 2011, he worked with the Department of Electrical and Computer Engineering, National University of Singapore, Singapore, as a Research Fellow. From 2016 to 2017, he worked with the Department of Electrical and Computer Engineering, University of Illinois at Urbana-Champaign, Champaign, IL, USA, as a Visiting Scholar. He joined the China University of Mining and Technology, Xuzhou, China, in 2019, where he is currently a Full Professor.
He is a Fellow of the Applied Computational Electromagnetics Society (ACES). He has authored or coauthored more than 150 refereed journal and conference papers. His current research interests include spoof surface plasmon polaritons theory and its applications, RF/Microwave antenna and filter design, computational electromagnetics, and microwave absorber theory and design. Dr. Zhao serves as an Associate Editor for IEEE Access and ACES Journal, and a Reviewer for multiple journals and conferences, including IEEE Transactions on Microwave Theory and Techniques, IEEE Transactions on Antennas and Propagation, IEEE Antennas and Wireless Propagation Letters, and other primary electromagnetics and microwave related journals.

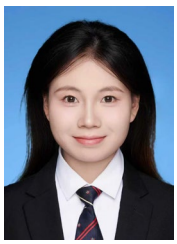

Yun Zhou, born in 2001 in Shandong, China, is currently pursuing her master's degree in Electronic Science and Technology at China University of Mining and Technology.
Her research interests include microwave absorbers, frequency selective surfaces.

Zhongxiang Shen (Fellow, IEEE) received the B.Eng. degree in electrical engineering from the University of Electronic Science and Technology of China, Chengdu, China, in 1987, the M.S. degree in electrical engineering from Southeast University, Nanjing, China, in 1990, and the Ph.D. degree in electrical engineering from the University of Waterloo, Waterloo, Ontario, Canada, in 1997.
From 1990 to 1994, he was with Nanjing University of Aeronautics and Astronautics, China. He was with Com Dev Ltd., Cambridge, Canada, as an Advanced Member of Technical Staff in 1997. He spent six months each in 1998, first with the Gordon McKay Laboratory, Harvard University, Cambridge, MA, and then with the Radiation Laboratory, the University of Michigan, Ann Arbor, MI, as a Postdoctoral Fellow. From January 1999 to December 2023, he was a Faculty Member (an Assistant Professor, an Associate Professor, and a Full Professor) of Nanyang Technological University, Singapore. He is now a Strategic Scientist at Yangtze Delta Region Academy of Beijing Institute of Technology, Jiaxing, Zhejiang, China. He has authored more than 240 journal papers (among them 180 were published in IEEE Journals) and also presented nearly 200 papers at international conferences. His research interests include small and planar antennas for various wireless communication systems, analysis and design of electromagnetic selective structures, hybrid numerical techniques for modeling RF/microwave components and antennas.
Dr. Shen served as the Chair of the IEEE MTT/AP Singapore Chapter in 2009. From January 2010 to August 2014, he was the Chair of IEEE AP-S Chapter Activities Committee. From July 2014 to December 2018, he served as the Secretary of IEEE AP-S. He was an elected AdCom member of the IEEE AP-S from January 2017 to December 2019. He served as an Associate Editor of the IEEE Transactions on Antennas and Propagation from July 2016 to July 2022. From January 2021 to December 2023, he is a Distinguished Lecturer of the IEEE AP-S. He is currently the Editor-in-Chief of IEEE Open Journal of Antennas and Propagation.